Mesoporous silica-coated silver nanoparticles as ciprofloxacin and siRNA co-delivery multifunctional platform for accelerated infected wound healing

Qiqi Liu
Shenzhen University
Ying Zhang
Longgang District People's Hospital of Shenzhen and The Second Affiliated Hospital of the ChineseUniversity of Hong Kong
Jingkai Huang
Southern University of Science and Technology Hospital
Zhourui Xu
Shenzhen University
Xiang Li
Shenzhen University
Jingyu Yang
Shenzhen University
Haoqiang Huang
Shenzhen University
Shiqi Tang
Shenzhen University
Yujuan Chai
Shenzhen University
Jinbo Lin
Longgang District People's Hospital of Shenzhen and The Second Affiliated Hospital of the ChineseUniversity of Hong Kong
Chengbin Yang (cbyang@szu.edu.cn)
Shenzhen University
Jia Liu
Longgang District People's Hospital of Shenzhen and The Second Affiliated Hospital of the ChineseUniversity of Hong Kong
Suxia Lin
The University of Hong Kong-Shenzhen Hospital

Research Article

Keywords: Mesoporous silica, siRNA, Synergistic therapy, Antibacterial, Skin infection, Wound healing

Posted Date: July 1st, 2022

DOI: https://doi.org/10.21203/rs.3.rs-1777499/v1

Abstract

The colonization of bacterial pathogens is a major concern in wound infection and becoming a public health issue. Herein, a core-shell structured Ag@MSN (silver core embedded with mesoporous silica, AM)-based nanoplatform was elaborately fabricated to co-load ciprofloxacin (CFL) and tumor necrosis factor-α (TNF-α) small interfering RNA (siTNF-α) (AMPC@siTNF-α) for treating the bacterial-infected wound. The growth of bacterial pathogens was mostly inhibited by released silver ions (Ag^+) and CFL from AMPC@siTNF-α. Meanwhile, the loaded siTNF-α was internalized by macrophage cells, which silenced the expression of TNF-α (a pro-inflammatory cytokine) in macrophage cells and accelerated the wound healing process by reducing inflammation response. In the *in vivo* wound model, the *Escherichia coli (E. coli)*-infected wound in mice almost completely disappeared after treatment with AMPC@siTNF-α, and no suppuration symptom was observed during the course of the treatment. Importantly, this nanoplatform had negligible side effects both *in vitro* and *in vivo*. Taken together, this study strongly demonstrates the promising potential of AMPC@siTNF-α as a synergistic therapeutic agent for clinical wound infections.

Introduction

Wounds could be caused by cut, burn, disease (e. g. diabetes), and surgical treatments [1, 2]. Unfortunately, these wounds can be easily contaminated by different pathogens, especially bacteria. These bacteria produce endotoxins and promote the expression of pro-inflammatory cytokines, such as tumor necrosis factor-α (TNF-α), which eventually lead to extended wound inflammation [3]. Currently, antibiotics are the major strategy for the treatment of infected wound infection [4, 5]. However, the overuse of antibiotics can cause the rapid proliferation of drug-resistance bacteria, which seriously impede the wound healing process. Therefore, it is urgent to develop a novel antibacterial strategy to prevent the formation of drug-resistance bacteria and promote wound rapid healing.

With the emergence of nanotechnology, nanoparticles (NPs) are considered as promising alternatives to traditional antibiotics, owing to their bactericidal activity, excellent biocompatibility, and broad-spectrum antibacterial properties [6–9]. Among them, silver (Ag) NPs have attracted great attention due to their strong and extensive antibacterial activity [10]. However, fast ions release and poor stability limit their applications [10]. Attaching or embedding Ag NPs into organic/inorganic matrix is an excellent strategy to endow them with enhanced colloidal stability. Of widely studied biocompatible nanomaterials, mesoporous silica NPs (MSNs) have been actively used as coating layers and drug reservoirs depending on their porous structure, adjustable pore size, large specific surface area, and versatile surface modification [11, 12]. Therefore, the integration of Ag NPs and MSNs (AM) can avoid the aggregation of Ag NPs and undesirable burst release of Ag, so as to effectively and safely treat wound bacterial infection. In addition, the drug loading ability of MSNs shell can be further used in synergistic antibacterial therapy. Wang et al. [13] constructed a nanoplatform of AM loaded with levofloxacin (LEVO) to treat drug-resistant bacterial infections and found that the nanoplatform could significantly reduce the infection through the synergistic antibacterial effect of Ag and LEVO. Similarly, Lu et al. [14] prepared the AM loaded with chlorhexidine (AMC), and indicated that the bacterial growth inhibition of the group

treated with AMC was about 20% higher than that of the group with AM. Ciprofloxacin (CFL) is a new kind of quinolones broad-spectrum antibacterial drugs for Gram-positive and negative bacteria [15]. And CFL has a zwitterionic molecular structure and can be loaded into the MSNs through electrostatic interaction [16]. Accordingly, it was believed that AM loaded with CFL would have the potential synergistic antibacterial properties.

In the stage of wound inflammation, the expression of some pro-inflammatory cytokines, especially TNF-α, is up-regulated [17]. Some studies have confirmed that high levels of TNF-α were closely related to the wound microenvironment, which could directly lead to the emergence of chronic wounds [18–20]. Considering the adverse effects of antibiotics, gene therapy, as a safe and effective method, has gradually attracted people's attention. Small interfering RNA (siRNA) is an important gene-silencing technique in gene therapy, which can specifically knock down the expression of target genes by mediating the degradation of target mRNA [21–23]. *TNF-α* gene can be silenced by a synthetic siRNA with complementary sequences. For example, intestinal inflammation was alleviated by delivering siTNF-α to inhibit TNF-α expression [24]. However, some factors limit the biomedical utility of the synthetic siRNAs, such as the negative charge, instability in the blood circulation, and immunogenicity [25, 26]. Therefore, it is urgent to exploit an ideal vector that can protect siRNA from degradation and inhibit the TNF-α gene's expression to achieve a better wound healing effect.

In this work, Ag@MSN encapsulated with PEG-g-PEI (AMP) was prepared to load CFL and siTNF-*α* (AMPC@siTNF-α) for promoting wound healing by synergistic inhibition of bacterial proliferation (Scheme 1). *In vitro*, the released CFL and silver ions (Ag^+) from AMPC@siTNF-α could enhance the bactericidal effect. The intracellular siTNF-α could down-regulate *TNF-α* expression of macrophage cells, which was expected to inhibit the pro-inflammatory response. *In vivo*, the fabricated antibacterial nanoplatform showed excellent bacteria-killing activity, promoting wound healing, and low biotoxicity in an *E. coli*-infected mouse wound model. Therefore, the multifunctional nanoplatform, AMPC@siTNF-α, might be a promising wound dressing for skin infection treatment depending on the synergistically bacterial-killing effect.

Materials And Methods

Materials

Cetyltrimethylammonium bromide (CTAB), absolute ethanol, silver nitrate solution ($AgNO_3$, ≥ 99.0%), formaldehyde (HCHO), branched PEG-g-PEI, ribonuclease A (RNase A), and 4',6-diamidino-2-phenylindole (DAPI) were purchased from Sigma-Aldrich Co., Ltd (St. Louis, MO, USA). Sodium hydroxide solution (NaOH), formaldehyde solution (37%), ethyl acetate (EA), and tetraethyl orthosilicate (TEOS) were obtained from Macklin Co., Ltd (Shanghai, China). Ammonium nitrate (NH_4NO_3) and CFL were from Aladdin Reagent Co., Ltd (Shanghai, China). Dulbecco's modified eagle's medium (DMEM), luria-bertani (LB) broth, penicillin-streptomycin solution, phosphate-buffered saline (PBS), fetal bovine serum (FBS), and lipofectamine™ 3000 (Lipo3000) were purchased from Gibco (Thermo Fisher, USA). Cell Counting

Kit-8 (CCK-8) and lipopolysaccharide (LPS) were from Biosharp Co., Ltd (Beijing, China). siTNF-α, Cy3-siRNA-negative control (Cy3-siNC) was synthesized by Shanghai GenePharma Co., Ltd. (Shanghai, China). Trypsinization (0.25%, without EDTA) was obtained from Solarbio Biotech Co., Ltd (Beijing, China). TRIcom reagent was from TIANMO BIOTECH Co., Ltd (Beijing, China). Evo M-MLV RT kit was purchased from Accurate Biology Co., Ltd (Hunan, China). Stormstar Sybr Green qPCR Master Mix was from DBI Bioscience Co., Ltd (Shanghai, China). Mouse TNF-α ELISA kit was purchased from Abcam (ab208348, UK). *Escherichia coli* (*E. coli*, CMCC44103) and *Staphylococcus aureus* (*S. aureus*, ATCC6538P) were obtained from the China General Microbiological Culture Collection Center.

Preparation of PEG-g-PEI-modified mesoporous silica-coated silver (AMP)

AM was prepared as described Song et al. [27] and Wang et al. [13] with minor modifications. Firstly, 0.3 mL of NaOH aqueous solution (2 M) and 0.1 g of CTAB were added to 50 mL of deionized water for incubation at 37°C for 30 min. And then, 0.3 mL of HCHO solution (1 M) and 1 mL of $AgNO_3$ solution (0.1 M) were added under stirring. Subsequently, 0.5 mL of TEOS was dropped into the reactive mixture. All the ingredients were then continuously stirred at 80°C and refluxed for 2 h. The resultant precipitate was collected via centrifugation at 8000 rpm for 10 min and washed with ethanol for three times. In order to remove the surfactant template CTAB, 0.06 g of NH_4NO_3 was added to the NPs dispersed in 60 mL of ethanol solution under a sonic bath for 2 h. After drying for 120 min at 60°C, the AM was obtained without the template. And then, 10 mg of AM was dissolved in 10 mL of deionized water, and 0.5 mL of PEG-g-PEI solution (100 mg/mL) was dropped into the solution under stirring (300 rpm/min, 25°C) overnight. Finally, AMP (1 mg/mL) was obtained through centrifuging at 12000 rpm/min for 15 min, discarding the supernatant, and washing the precipitation with deionized water for three times to remove the excess PEG-g-PEI.

Ciprofloxacin loading by AMP

In order to load CFL into drug carriers, AMP (5 mg) was mixed with CFL aqueous solution (500-4000 μg/mL, 5 mL) under stirring overnight at 25°C. Then, the mixture was separated by centrifugation (8000 rpm/min, 5 min) and washed several times until there was no free CFL in the supernatant. The amount of free CFL in the supernatant was calculated from a calibration curve based on the absorbance intensity at 275 nm by UV-vis (TP-720 spectrometer, Tianjin Tuopu Instrument Co., Ltd). The percentage of CFL loading into AMP was calculated as follows:

$$\mathrm{LE}\ (\%) = \frac{m_{\mathrm{oriCFL}} - m_{\mathrm{supCFL}}}{m_{\mathrm{AMP}} + m_{\mathrm{oriCFL}}} \times 100\%$$

Where the m_{oriCFL}, m_{supCFL}, and m_{AMP} represent the mass of original CFL, CFL in the supernatant, and AMP, respectively. The LE represents the loading efficiency.

Drug release from AMP loaded with CFL (AMPC)

To detect the release of CFL from AMPC, the AMPC (2 mg) were dispersed in PBS (pH 7.4, 2 mL) and transferred into a dialysis bag with a molecular weight cut-off of 1000 Da and kept in PBS (50 mL) on a shaking table at 37°C for 48 h. After 2 mL of the solution was removed at different time points, the drug release efficiency was measured by UV-vis at 275 nm. In order to keep the solution volume constant, 2 mL of fresh PBS needed to be added after each sampling.

To study the release of Ag from AMPC, the AMPC was suspended in an LB culture medium. After the mixture was incubated at 37°C, the UV-vis adsorption of the AMPC solution was monitored over a time period. The amount of consumed Ag was detected at 417 nm using a microphone reader (Bio-teak, Epoch-2).

Preparation and characterization of AMP loaded with siRNA (AMP@siRNA)

First, AMP and siNC (sense: 5'-CGAAGUGUGUGUGUGUGGC-3', antisense: 5'-GCCACACACACACACUUCG-3') with different weight ratios (0:1, 7.5:1, 15:1, 30:1, 60:1, and 120:1) were mixed at 25°C for 30 min. and then the binding capacity was evaluated by the agarose gel electrophoresis (110 V, 8 min), the gel was imaged under a UV transillumination (FlourChem E, ProteinSimple, San Jose, CA, USA) and the gray value was calculated by Image J (Bethesda, Maryland, USA). The zeta potential and hydrodynamic diameter of AMP@siNC were then measured by Zetasizer Nano-ZS90 (Malvern Panalytical, Ltd). Their morphological properties were detected by transmission electron microscopy (TEM, HT7700, Hitach, Ltd).

Serum enzymatic protection test

To determine the ability of AMP to protect siRNA from RNase A, the AMP and siNC (weight ratio of 15:1) were incubated at a 2 μL of RNase A (0.5 μg/mL) for 0, 5, 10, 15, 20, 25, and 30 min respectively. Subsequently, the solution was mixed with 1% SDS at 4°C for 3 min. Then the remaining siRNAs were detected by agarose gel electrophoresis (110 V, 8 min) and quantified based on the fluorescence intensity.

The cytotoxicity and hemolysis assay of AMP

To evaluate the cytotoxicity of AMP *in vitro*, 100 μL of RAW 264.7 cells with a density of 5000 cells/well were seeded into 96-well plates. After culturing for 24 h, AMP with different concentrations (5, 10, 20, 40, 60, 80, 100, 120, and 140 ppm) were placed in the wells and co-cultured for another 24 h. Then, the culture medium was removed, and the wells were washed twice with PBS. For each well, 100 μL of 10% CCK-8 solution diluted in culture medium was added, and the plate was incubated in an incubator (37°C, 5% CO_2) for 1 h. Subsequently, the cell viability was measured at the absorbance of 450 nm by a microplate reader (Bio-teak, Epoch-2) and calculated according to the following formula:

$$\text{Cell viability (\%)} = \frac{A_{eg} - A_{bg}}{A_{ng} - A_{bg}} \times 100\%$$

Where A_{bg} and A_{ng} represent the absorbance of cell- and AMP-free medium with CCK-8 solution, respectively. A_{eg} represents the absorbance of medium with cells, CCK-8, and AMP solution.

To investigate the hemolytic effects of AMP to red blood cells (RBCs), 500 μL of blood was diluted 10-fold with PBS. The blood was mixed gently and centrifuged at 10000 g for 5 min. The supernatant was discarded, and RBCs were washed a few times by suspending them in a PBS solution (pH 7.4) until the supernatant was clear. Finally, RBCs were resuspended with 10 mL of PBS. To evaluate the hemolytic effects, 200 μL of RBCs were incubated with 800 μL of H_2O (as positive control), 800 μL of PBS (as negative control), and AMP with different concentrations for 4 h in a 37 °C incubator. After incubation, the samples were further centrifugated at 10000 g for 5 min, and 100 μL of supernatants were extracted to quantify hemoglobin by recording the absorbance at 577 nm. The percentage of hemolysis rate was calculated as follows.

$$\text{Hemolysis rate (\%)} = \frac{A_{sam} - A_{neg}}{A_{pos} - A_{neg}} \times 100\%$$

Where the A_{sam}, A_{neg}, and A_{pos} represent the absorbance value of treatment, negative and positive groups, respectively.

siRNA transfection

RAW264.7 cells were cultured in DMEM medium supplemented with 10% FBS, 1% penicillin (100 μg/mL), and streptomycin (100 μg/mL) in an atmosphere with 5% CO_2 at 37°C. Subsequently, RAW264.7 cells were seeded onto 24-well plates with a density of 3×10^4 cells/well, and cultured for 24 h. And then, cells were activated with 1 μg/mL of LPS. After 4 h, the maintenance medium was replaced with serum-free DMEM. Meanwhile, the AMP (1 mg/mL) and Cy3-siNC (100 pM) were mixed at a weight ratio of 15:1 and 30:1 at 25°C for 40 min. Then, the above AMP@siNC were added to the 24-well plates and incubated for 4 h.

To examine the uptake efficiency, these cells were imaged using fluorescent microscopy and assessed by flow cytometry, respectively. Additionally, to study the gene *TNF-α* expression, some cells were cultured for 72 h post-transfection in DMEM medium with 10% FBS after removing the old medium-containing

material. The sense and antisense sequences of siTNF-α were listed as follows: sense: 5'-GUCUCAGCCUCUUCUCAUUdTdT-3', antisense: 5'- AAUGAGAAGAGGCUGAGACdTdT-3'.

Fluorescence imaging and siRNA transfection efficiency

After being treated with AMP@siNC for 4 h, cells were washed three times with PBS (pH 7.4) and fixed with 4% formaldehyde for 15 min. Cells were then stained with DAPI for 20 min. The filters of the inverted microscope were set for DAPI (excitation at 405 nm and the emission was collected with a 450/50 nm band pass filter) and Cy3 (excited with 543 nm and emission was collected with a band pass filter 605/50 nm). To quantify cell internalization, the post-transfection cells were washed three times with PBS and collected by trypsinization (0.25%, without EDTA). Cy3 was used as a fluorescent marker (filter set for ECD was applied) to quantify the fluorescence intensity. The samples were evaluated by a flow cytometer (CytoFLEX, Beckman).

Anti-inflammatory activity of AMP@siTNF-α

To demonstrate the anti-inflammatory, LPS-activated macrophages were used to elicit the release of the inflammatory mediator TNF-α [28, 29]. The transcription level of *TNF-α* gene was investigated by qRT-PCR according to previous experiences [30]. In brief, the total RNA from RAW264.7 cells was extracted using a TRIzol reagent (Invitrogen) and quantified using a micro-spectrophotometer (Epoch2, Biotek Instruments). Total RNA (800 ng) was reverse-transcribed to cDNA using PrimeScriptTM RT reagent Kit (AG11705, Aikerui Biological Engineering Co., Ltd, Hunan, China). The mRNA level of *TNF-α* gene was measured by qRT-PCR using the SYBR green dye (DBI-Bioscience 2143) in a QuanStudio 1 applied biosystem. The qRT-PCR was performed in a 20 μL reaction volume containing SYBR Premix Ex Taq II (10 μL), forward prime (10 μM, 0.8 μL), reverse primer (10 μM, 0.8 μL), cDNA template (5 ng/μL, 2 μL), and ddH_2O (6.4 μL). The PCR conditions were denaturation at 95°C for 30 s, followed by 40 cycles of amplification (95°C for 5 s, 60°C for 30 s). The melting curves were measured at 95°C for 5 s and 60°C for 1 min. The *β-actin* gene was used as the internal control reference gene. Finally, gene expression was calculated using the $2^{-\Delta\Delta Ct}$ method [31]. The primer sequences were as follows: β-actin F: 5'-GGTCATCACCATTGGCAATG-3', R: 5'-TAGTTTCGTGGATGCCACAG-3'; TNF-α F: 5'-GTCTGGGCAGGTCTACTTTGG-3', 5'-GGTTGAGGGTGTCTGAAGGAG-3'. Furtherly, TNF-α content in the cell-free supernatants was determined using the TNF-α ELISA kit according to the manufacturer's instructions.

In vitro antibacterial activity of AMPC

The minimum inhibitory concentrations (MICs) of the different NPs for *E. coli* and *S. aureus* were determined by a micro broth dilution method. The strains were cultured in LB medium at 37°C to the logarithmic phase. And then, the bacterial fluid was diluted to a concentration of 5×10^5 colony-forming units per mL (CFU/mL). Subsequently, AM, AMP, and AMPC were separately added into tubes with 4 mL of bacterial cultures and shaken for 24 h at 37°C. After naked eye observation, the lowest concentration of the NP in the tube without bacteria growth was determined as MIC.

To further evaluate the antibacterial activity of these NPs, *E. coli* and *S. aureus* in the exponential phase were serially diluted with LB medium to a concentration of 5×10^5 CFU/mL. Then, the bacterial suspension was added to 96-well plates and treated with AM, AMP, and AMPC (50 μg/mL). At different time intervals, the OD_{600} of bacterial suspensions was determined using a microphone reader (Bio-teak, Epoch-2) to obtain killing curves. Additionally, after incubation at 37°C for 12 h, 10 μL of the diluted bacterial solution was spread on LB agar plates. After incubation at 37°C for another 12 h, digital images of each plate were captured, and the CFU/mL and antibacterial ratio were obtained. CFU/mL was calculated according to the following equation respectively:

$$\mathrm{CFU/mL} = \frac{\text{colonies' number} \times \text{dilution ratio}}{\text{plated volume}}$$

In vivo wound healing and safety evaluation

The *in vivo* antibacterial efficacy of AMPC@siTNF-α was examined on the *E. coli* infection model in terms of wound recovery and histological analysis. All experiments involving animals were approved by the Institutional Animal Ethical Committee at the Laboratory Animal Research Center at Shenzhen University (Shenzhen, China). Briefly, 6-8-week-old BALB/c mice (18-22 g) were obtained from Guangdong Medical Laboratory Animal Center (Guangdong, China). Mice were anesthetized by intraperitoneal injection of 4% pentobarbital sodium (1.0 mL/kg). Round skin wounds were created on the back with a biopsy puncture of 8 mm diameter, and then 10 μL of *E. coli* suspension (10^7 CFU/mL) was added to the wound surface. One day later, 200 μL of AM, AMP, AMPC, AMP@siTNF-α, and AMPC@siTNF-α suspensions in PBS (50 μg/mL) were placed on the wounds. The wounds were treated with PBS and levofloxacin (LEVO) as the negative and positive controls, respectively. The area and images of the wound were recorded from 0 to 12 days. After 12 days of treatment, wound tissues were collected and dipped in fixative (4% paraformaldehyde). Wound tissues were sectioned and stained at Wuhan Service Biotechnology Co., Ltd., and the images were then recorded and analyzed using a Pathology Sectioning Scanner (LEICA-Aperio, carbon disulfide).

Statistical analysis

All experiments were conducted at least three times, and the data were shown as mean ± standard deviation (SD). *T*-test were used to evaluate the significance of different data. It was considered as statistically significant when $p < 0.05$ (*), $p < 0.01$ (**), and $p < 0.001$ (***).

Results And Discussion

Preparation and characterization of AMP@siRNA

According to previous reports [32, 33], AMP was obtained by modifying AM with PEG-g-PEI. The prepared AM showed a uniform and monodispersed spherical morphology with a typical core-shell structure, in which Ag was embedded in the center of the mesoporous silica shell layer. Compared with the morphology of AM, a layer of material wrapped on the surface of AMP could be clearly observed in **Fig. 1A**. The dynamic light scattering (DLS) results indicated the hydrodynamic diameter of AM and AMP is 123 nm and 146 nm, respectively (**Fig. 1B**). The narrow size distribution indicated that these NPs have excellent size uniformity. The absorption peaks of AM and AMP in the UV-vis spectrum were at about 417 nm (**Fig. 1C**). The changes in morphology and average size indicated that PEG-g-PEI has been successfully decorated on AM surface.

Furthermore, the siRNA loading efficiency was evaluated by agarose gel electrophoresis. The results indicated that when the weight ratio of AMP and siNC went up to 15:1, no free siRNA was observed in the agarose gel, meaning that all siRNA had been retarded by AMP in the sample wells (**Fig. S1 A**). Thus, the optimal weight ratio of AMP and siRNA was fixed at 15:1. Subsequently, the surface zeta potential of AMP@siNC gradually rised with an increased weight ratio of AMP and siNC (**Fig. 1D**). The zeta potential of AMP@siNC was reversed from -2.87 ± 0.35 mV (weight ratio at 7.5:1) to 30.63 ± 0.74 mV (weight ratio at 240:1), which would help the loaded siRNA cross the negatively charged cell membrane to the cytoplasm [34]. As a siRNA carrier, it is important to protect siRNA from serum nuclease degradation. Firstly, siNC was incubated in deionized water containing RNase A for a different time at 37°C, and the results showed that the brightness of the remnant siNC bands gradually darkened with extended incubation time. When the incubation time was 18 min, the brightness disappeared completely, indicating that siNC was completely degraded by RNase A (**Fig. S1Bi**). Then, the AMP@siNC (weight ratio at 15:1) were incubated at the same concentration of RNase A solution for the same time, followed by the separation of loaded siNC from AMP@siNC using SDS. Results indicated that siNC had no noticeable degradation under the protection of AMP (**Fig. S1Bii**). In addition, quantitative analysis of siNC degradation revealed that naked siNC was obviously degraded by RNase A, and AMP could well protect siNC from degradation (**Fig. 1E**). These results indicated that AM could be protonated by PEG-g-PEI to form AMP, which can carry siRNA and protect siRNA from degradation.

The loading and release of antibiotic and silver ion

The loading efficiency and release behavior of CFL in AMP were carefully evaluated by fluorescence spectrophotometer. The pure CFL displayed a characteristic absorption peak at 275 nm. The intensity of the absorption peak of CFL increased, accompanied by the higher concentration of CFL (**Fig. S2 A**, **B**). In order to obtain the encapsulation and loading rates of CFL, AMP was mixed with CFL at different mass ratios. When the mass ratio of CFL and AMP was between 1:1 and 3:1, the encapsulation and loading efficiencies of CFL increased significantly from 22% to 65%, 23% to 64%, respectively. When CFL: AMP (w:w) was 4:1, the maximum encapsulation and loading efficiencies both reached the maximum value of 69% (**Fig. S3**, **Fig. 2A**), which was higher than that of Au NPs loaded-CFL (60%, 34%) [35] and fibrin NPs loaded-CFL (52%, 0.59%) [36]. The release behaviors of CFL from AMPC *in vitro* were also tested in PBS (pH 7.4) at 37°C for 48 h. A rapid release happened in the first 8 h, reaching 34%. In the following stage, a

prolonged release profile occurred in the next 8 h to 48 h and stabilized after 48 h, with a maximum release percentage of 41% (**Fig. 2B**).

The release profiles of Ag from AMPC *in vitro* were performed indirectly by culturing AMPC in an LB medium at 37°C. The UV-vis spectrum showed that the absorption peak intensity at 417 nm gradually decreased over time (**Fig. 2C**). The change of Ag^+ content was determined by standard curve UV-vis absorbance (**Fig. S2 C**). The cumulative consumption of Ag from AMPC was improved along with the increase of the NP concentration. When the concentration of AMPC was 200 μg/mL, Ag release increased rapidly in the first 12 h and then remained saturated in the following 12 to 50 h, with a maximum release of 35 μg/mL (**Fig. 2D**). This may be attributed to the oxidative chelation process, which converted AMPC into Ag^+ through various salts and peptides in the LB medium [13, 37]. Moreover, some peptides (e. g., glutathione) are also common in natural bacterial biofilms, which will enhance the release of Ag^+ in the infectious wound environment [38, 39].

Biosafety evaluation of AMP

It is necessary to evaluate NPs biosafety for their biological application. In the study, the toxicity of AMP was tested by co-culturing with RAW264.7 cells. Results indicated approximately 90% of cells remained alive after treatment with different concentrations of AMP, which indicated that AMP was not toxic to RAW264.7 cells (**Fig. S4**). Furthermore, in order to ensure that the NPs did not hemolyze in the blood *in vivo*, the hemolytic effect of AMP was evaluated. It could be found that there was no hemolysis at the concentration of 0-32 μg/mL, while hemolysis gradually appeared when the concentration was higher than 32 μg/mL (**Fig. S5**). The safe concentration (16 μg/mL) was confirmed and adopted in the following study.

Intracellular uptake and transfection efficiency of siRNA

To demonstrate the siRNA delivery efficiency of the AMP, RAW264.7 cells were treated with AMP@siRNA, in which the siRNA was labeled with Cy3, and the intracellular fluorescence signal was monitored by an inverted fluorescence microscope. Non-treated, AMP, and naked Cy3-siRNA were used as the negative controls, while the commercialized siRNA transfection reagent, Lipo3000, served as the positive control. No Cy3 fluorescence signals (red) were observed from cells in the negative controls. In contrast, significant intracellular Cy3 fluorescence was observed in AMP@siRNA- and Lipo3000/siRNA-treated groups (**Fig. 3A**). Furthermore, quantitative analysis by flow cytometry revealed that the transfection efficiency (87.57%) of the group treated with AMP@siRNA at 30:1 (w:w) was almost the same as that (87.71%) of the positive control (**Fig. 3B**). And its mean fluorescence intensity was about 2-fold higher than that of the positive control (**Fig. S6**). These results clearly suggested that AMP could be employed as an efficient carrier for intracellular siRNA delivery in macrophage cells.

Gene silence efficiency of AMP@siTNF-α on LPS induced-macrophages

The efficiency of AMP-mediated siTNF-α delivery to knockdown TNF-α expression was evaluated by qRT-PCR. In LPS-induced RAW264.7 cells, the transcription level of TNF-α mRNA was up-regulated by 5.3-fold and the secreted TNF-α protein in medium supernatant increased by 3-fold compared with non-treated cells (**Fig. S7**, **Fig. 3D**). After being treated with AMP and AMP@siNC, the expression of TNF-α mRNA and protein decreased significantly, by 1.6-fold, which might be related to the anti-inflammatory properties of the released Ag [40, 41]. Moreover, their expression decreased most significantly (12.4-fold) in the group treated with AMP@siTNF-α than that of the positive (Lipo3000@siTNF-α) control (2.3-fold) (**Fig. S7**, **Fig. 3D**). This indicated that siTNF-α was successfully and efficiently transfected to cells.

Antibacterial activity of AMPC on *E. coli* and *S. aureus*

To evaluate the *in vitro* antibacterial activity of different NPs, as Gram-negative and positive representative bacteria, *E. coli* and *S. aureus* were selected as a model, respectively [42]. The MICs of different NPs against the two bacteria were measured. The MICs of AM for *E. coli* and *S. aureus* were confirmed at 80 μg/mL and 120 μg/mL, respectively (**Fig. 4A**, **Fig. S8**), which were comparable with the previous reports [14, 43]. The antibacterial ability of AM is related to the cell wall composition of the two bacteria. The wall of Gram-positive bacteria is mainly composed of peptidoglycan, which is more tenacious and can protect the plasma membrane from the attack of NPs. In addition, the wall of Gram-negative bacteria is mainly composed of peptidoglycan, lipoprotein, and phospholipid layer, which is relatively loose [44, 45]. The MICs of AMP against both strains were the same as those for AM, indicating that PEG-g-PEI did not affect the growth of bacteria (**Fig. 4A**, **Fig. S8**). Moreover, after loading antibiotic CFL with AMP, the MICs (25 μg/mL) against *E. coli* and *S. aureus* decreased by 3.2-fold and 4.8-fold, respectively. This revealed that AMPC was more effective in the killing of *E. coli* and *S. aureus*, because the released Ag and loaded CFL played a synergistic antibacterial role.

According to the results of MICs, the different NPs with 50 μg/mL were chosen to explore their effect on anti-bacteria. After being cultured for 12 h at 37°C, different NPs-treated bacterial liquid was coated on culture plates, and then quantitative bacterial colony densities were also evaluated. There were no colonies formed after AMPC treatment. Compared with the control group, the AM- and AMP-treated groups had fewer colonies (**Fig. 4B**, **4C**, **Fig. S9**, **S10**). The growth curves also showed that the OD values of the controls increased almost linearly with the increase of culture time and reached about 0.6 when cultured for 12 h (**Fig. 4C**, **Fig. S10**). After treatment with different NPs, the treatment groups showed different degrees of inhibition of the two bacteria. Compared with the control, AM- and AMP-treated groups, in the whole culture process, the AMPC-treated group showed stronger antibacterial ability, and the OD value was the lowest (about 0) at 12 h (**Fig. 4D**, **Fig. S11**). In addition, after different treatments, the antibacterial ratio was also measured. The antibacterial ratio of the AMPC-treated groups reached 100%, demonstrating the excellent synergistic antibacterial effect of AMPC (**Fig. 4E**, **Fig. S12**).

Efficiency of the AMPC@siTNF-α in promoting wound healing

Bacterial infection is the most severe interference factor in impeding wound healing. Excessive inflammation will destroy the residual epithelial tissue, resulting in collagen metabolism disorder and

wound festering [46]. To evaluate the therapeutic effect of AMPC@siTNF-α *in vivo*, as illustrated in **Fig. 5A**, after the establishment of the wound model infected by *E. coli*, different NPs were placed on the wound surface. The whole course of treatment was completed within 12 days. As shown in **Fig. 5B** and **Fig. 5C**, the wounds in the control group showed obvious inflammation during the treatment. In contrast, the wound treated with AMPC@siTNF-α had no inflammation, scabs were formed after 8 days of treatment, and the wound healing completed close to 100% after 12 days, similar to the positive control (LEVO-treated). Remarkably, the AMPC@siTNF-α treatment exhibited the best wound healing effect. Furthermore, no weight loss was observed in all groups throughout the course, eliminating the security concern to the AMPC@siTNF-α (**Fig. 5D**).

H&E staining was used to evaluate the infected tissues after 12 days of treatment. The groups treated with AMPC and AMPC@siTNF-α showed almost complete healing as indicated by the relatively loose arrangement of collagen fibers, the less proliferation of fibrous tissue, and the more sebaceous glands, which were the same as the normal skin. For unhealed wounds, the tissue contained large numbers of fibroblasts with regularly arranged. The groups with no treatment, AM, AMP, AMPC, and AMP@siTNF-α showed similar fibroblast arrangements (**Fig. 5E**). These results indicated that AMPC@siTNF-α could rapidly promote wound healing through the synergistic effect of released CFL and siTNF-α.

In addition, the main organs (heart, liver, spleen, lung, and kidney) of the treated mice were further analyzed by H&E staining (**Fig. S13**). No obvious pathological changes and organic damage were found in the pathological section. In conclusion, these results strongly indicated that the treatment strategy based on AMPC@siTNF-α not only effectively promoted wound healing, but also had good biosafety *in vivo*.

Conclusions

In conclusion, a multifunctional nanoplatform of AMPC@siTNF-α has been successfully fabricated and proved to be effective for the treatment of *E. coli*-infected wounds both *in vitro* and *in vivo*. The combination of the inner Ag core and the mesoporous silica shell displays the controlled release of Ag^+, antibiotics, and siRNA simultaneously. AMPC exhibits superior antibacterial activity *in vitro* due to its synergistic effect between Ag^+ and CFL. AMP@siTNF-α can be efficiently internalized by macrophages and significantly reduce the expression of the pro-inflammatory factor TNF-α *in vitr*o. In the *in vivo* wound infection model, the *E. coli* infected wound rapidly disappears after treatment with AMPC@siTNF-α, which is 6-fold faster than that of the negative control and 2.5-fold faster than that of the single treatment group (AMPC- and AMP@siTNF-α-treated). Importantly, the nanoplatform has negligible toxicity with negligible side effects on mice during the test. This study strongly indicates a promising potential of AMPC@siTNF-α as a synergistic and safe therapeutic agent for clinical wound infections.

Declarations

Acknowledgments

We thank the Instrument Analysis Centre of Shenzhen University for its assistance with imaging analysis.

Author Contributions

Conceived and designed the experiments: S.X.L, J.L. and C.B.Y. Performed the experiments and collected data: Q.Q.L, Y.Z., J.K.H, X.L., J.Y.Y., H.Q.H., and S.Q.T. Analysis data: Q.Q.L, Y.Z., S.X.L., J.B.L. and Z.R.X. Wrote the original manuscript: Q.Q.L, Y.Z., Revised the manuscript: S.X.L, J.L., Y.J.C. and C.B.Y. All authors have read and agreed to the published version of the manuscript.

Funding

This work was supported by the National Natural Science Foundation of China (81900264), the Natural Science Foundation of Guangdong Province (2019A1515012163), the University Stable Support Research Funding of Shenzhen (20200813153346001), Start-up Grant from Shenzhen University (2019136), the Shenzhen Science and Technology Innovation Commission (JCYJ20210324130609027) and the Longgang Medical and Health Science and Technology Project (LGKCYLWS2020040 and LGKCYLWS2021000010).

Availability of data and materials

The data are all available upon request.

Ethics approval and consent to participate

All animal experiments were performed in accordance with the guidelines and the ethical standards of the Institutional Animal Ethical Committee at the Laboratory Animal Research Center at Shenzhen University.

Consent for publication

All authors gave their consent for publication.

Competing interests

The authors declare no conflict of interest.

References

1. Sen CK. Human wounds and its burden: updated 2020 compendium of estimates. Adv Wound Care. 2021;10(5):281-92.
2. Simões D, Miguel SP, Ribeiro MP, Coutinho P, Mendonça AG, Correia IJ, et al. Recent advances on antimicrobial wound dressing: A review. Eur J Pharm Biopharm. 2018;127:130-41.
3. Guo SA, DiPietro LA. Factors affecting wound healing. J Dental Res. 2010;89(3):219-29.

4. Clatworthy AE, Pierson E, Hung DT. Targeting virulence: a new paradigm for antimicrobial therapy. Nat Chem Biol. 2007;3(9):541-48.
5. Paterson DL, Harris PNA. Colistin resistance: a major breach in our last line of defence. Lancet Infect Dis. 2016;16(2):132-33.
6. Hajipour MJ, Fromm KM, Ashkarran AA, de Aberasturi DJ, de Larramendi IR, Rojo T, et al. Antibacterial properties of nanoparticles. Trends Biotechnol. 2012;30(10):499-511.
7. Peng ZH, Zhang XC, Yuan L, Li T, Chen YJ, Tian H, et al. Integrated endotoxin-adsorption and antibacterial properties of platelet-membrane-coated copper silicate hollow microspheres for wound healing. J Nanobiotechnology. 2021;19(1):383.
8. Zhang Y, Yue TX, Gu WT, Liu AD, Cheng MY, Zheng HY, et al. pH-responsive hierarchical H_2S-releasing nano-disinfectant with deep-penetrating and anti-inflammatory properties for synergistically enhanced eradication of bacterial biofilms and wound infection. J Nanobiotechnology. 2022;20(1):55.
9. Wang W, Lu KJ, Yu CH, Huang QL, Du YZ. Nano-drug delivery systems in wound treatment and skin regeneration. J Nanobiotechnology. 2019;17(1):82
10. Lee SH, Jun BH. Silver nanoparticles: Synthesis and application for nanomedicine. Int J Mol Sci. 2019;20(4):865.
11. Wang Y, Zhao QF, Han N, Bai L, Li J, Liu J, et al. Mesoporous silica nanoparticles in drug delivery and biomedical applications. Nanomedicine. 2015;11(2):313-27.
12. Barkat A, Beg S, Panda SK, S Alharbi K, Rahman M, Ahmed FJ. Functionalized mesoporous silica nanoparticles in anticancer therapeutics. Semin Cancer Biol. 2021;69:365-75.
13. Wang Y, Ding XL, Chen Y, Guo MQ, Zhang Y, Guo XK, et al. Antibiotic-loaded, silver core-embedded mesoporous silica nanovehicles as a synergistic antibacterial agent for the treatment of drug-resistant infections. Biomaterials. 2016;101:207-16.
14. Lu MM, Wang QJ, Chang ZM, Wang Z, Zheng X, Shao D, et al. Synergistic bactericidal activity of chlorhexidine-loaded, silver-decorated mesoporous silica nanoparticles. Int J Nanomedicine. 2017;12:3577-89.
15. Cilliers P, Seldon R, Smit FJ, et al. Design, synthesis, and antimycobacterial activity of novel ciprofloxacin derivatives. Chem Biol Drug Des. 2019;94(2):1518-36.
16. Veclani D, Melchior A. Adsorption of ciprofloxacin on carbon nanotubes: Insights from molecular dynamics simulations. J Mol Liq. 2020;298:111977.
17. Nosenko MA, Ambaryan SG, Drutskaya MS. Pro-inflammatory cytokines and skin wound healing in mice. Mol Biol. 2019;53(5):741-54.
18. Park GT, Yoon JW, Yoo SB, Song YC, Song P, Hyoung-Kyu Kim HK, et al. Echinochrome a treatment alleviates fibrosis and inflammation in bleomycin-induced scleroderma. Mar Drugs. 2021;19(5):237.
19. Goldberg MT, Han YP, Yan CL, Shaw MC, Garner WL. TNF-alpha suppresses alpha-smooth muscle actin expression in human dermal fibroblasts: an implication for abnormal wound healing. J Invest

Dermatol. 2007;127(11):2645-55.

20. Lai JJ, Lai KP, Chuang KH, Chang P, Yu IC, Lin WJ, et al. Monocyte/macrophage androgen receptor suppresses cutaneous wound healing in mice by enhancing local TNF-alpha expression. J Clin Invest. 2009;119(12):3739-51.
21. Han H. RNA interference to knock down gene expression. Methods Mol Biol. 2018;1706:293-302.
22. Zhang XM, Lin ZL, Yang JY, Liu GL, Hu ZL, Huang HQ, et al. Carbon dioxide-derived biodegradable and cationic polycarbonates as a new siRNA carrier for gene therapy in pancreatic cancer. Nanomaterials. 2021;11(9):2312.
23. Yang Y, Qin Z, Zeng W, Tang T, Cao Y, Mei C, et al. Toxicity assessment of nanoparticles in various systems and organs, Nanotechnol Rev. 2017;6:279-89.
24. Wilson DS, Dalmasso G, Wang LX, Sitaraman SV, Merlin D, Murthy N. Orally delivered thioketal nanoparticles loaded with TNF-α-siRNA target inflammation and inhibit gene expression in the intestines. Nat Mater. 2010;9(11):923-28.
25. Zou Y, Sun XH, Wang YB, Yan CN, Liu YJ, Li J, et al. Single siRNA nanocapsules for effective siRNA brain delivery and glioblastoma treatment. Adv Mater. 2020;32(24):e2000416.
26. Huang YY, Zheng SQ, Guo ZX, de Mollerat du Jeu X, Liang XJ, Yang Z, et al. Ionizable liposomal siRNA therapeutics enables potent and persistent treatment of Hepatitis B. Signal Transduct Target Ther. 2022;7(1):38.
27. Song ZL, Ma YJ, Xia GG, Wang Y, Kapadia W, Sun ZY, et al. In vitro and in vivo combined antibacterial effect of levofloxacin/silver co-loaded electrospun fibrous membranes. J Mater Chem B. 2017;5(36):7632-43.
28. Pae HO, Oh GS, Choi BM, Shin S, Chai KY, Oh H, et al. Inhibitory effects of the stem bark of Catalpa ovata G. Don. (Bignoniaceae) on the productions of tumor necrosis factor-alpha and nitric oxide by the lipopolisaccharide-stimulated RAW 264.7 macrophages. J Ethnopharmacol. 2003;88(2-3):287-91.
29. Inpanya P, Faikrua A, Ounaroon A, Sittichokechaiwut A, Viyoch J. Effects of the blended fibroin/aloe gel film on wound healing in streptozotocin-induced diabetic rats. Biomed Mater. 2012;7(3):035008.
30. Yang CB, Chan KK, Lin WJ, Soehartono AM, Lin GM, Toh HT, et al. Biodegradable nanocarriers for small interfering ribonucleic acid (siRNA) co-delivery strategy increase the chemosensitivity of pancreatic cancer cells to gemcitabine. Nano Res. 2017;10(9):3049-67.
31. Livak KJ, Schmittgen TD. Analysis of relative gene expression data using real-time quantitative PCR and the $2^{-\Delta\Delta Ct}$ method. Methods. 2002;25(4):402-08.
32. Lu YX, Wu FP, Duan WH, Mu XL, Fang S, Lu NN, et al. Engineering a “PEG-g-PEI/DNA nanoparticle-in-PLGA microsphere” hybrid controlled release system to enhance immunogenicity of DNA vaccine. Mater Sci Eng C Mater Biol Appl. 2020;106:110294.
33. Rudolph C, Sieverling N, Schillinger U, Lesina E, Plank C, Thünemann AF, et al. Thyroid hormone (T3)-modification of polyethyleneglycol (PEG)-polyethyleneimine (PEI) graft copolymers for improved gene delivery to hepatocytes. Biomaterials. 2007;28(10):1900-11.

34. Zhang D, Wei L, Zhong ML, Xiao LH, Li HW, Wang JF. The morphology and surface charge-dependent cellular uptake efficiency of upconversion nanostructures revealed by single-particle optical microscopy. Chem Sci. 2018;9(23):5260-69.
35. Nawaz A, Ali SM, Rana NF, Tanweer T, Batool A, Webster TJ, et al. Ciprofloxacin-loaded gold nanoparticles against antimicrobial resistance: An in vivo assessment. Nanomaterials. 2021;11(11):3152.
36. Thattaruparambil Raveendran N, Mohandas A, Ramachandran Menon R, Somasekharan Menon A, Biswas R, Jayakumar R. Ciprofloxacin- and Fluconazole-Containing Fibrin-Nanoparticle-Incorporated Chitosan Bandages for the Treatment of Polymicrobial Wound Infections. ACS Appl Bio Mater. 2019;2(1):243-54.
37. Liong M, France B, Bradley KA, Zink JI. Antimicrobial activity of silver nanocrystals encapsulated in mesoporous silica nanoparticles. Adv. Mater. 2009;21(17):1684-9.
38. Jin Y, Yang YD, Duan W, Qu XT, Wu JM. Synergistic and on-demand release of Ag-AMPs loaded on porous silicon nanocarriers for antibacteria and wound healing. ACS Appl. Mater. Interfaces 2021;13(14):16127-41.
39. Tong CY, Zhong XH, Yang YJ, Liu X, Zhong GW, Xiao C, et al. Pb@Pda@Ag nanosystem for synergistically eradicating MRSA and accelerating diabetic wound healing assisted with laser irradiation. Biomaterials. 2020;243:119936.
40. Yilma AN, Singh SR, Dixit S, Dennis VA. Anti-inflammatory effects of silver-polyvinyl pyrrolidone (Ag-PVP) nanoparticles in mouse macrophages infected with live Chlamydia trachomatis. Int J Nanomed. 2013;8:2421-32.
41. Wong KK, Cheung SO, Huang L, Niu J, Tao C, Ho CM. Further evidence of the anti-inflammatory effects of silver nanoparticles. Chem Med Chem. 2009;4(7):1129-35.
42. Misic AM, Gardner SE, Grice EA. The wound microbiome: Modern approaches to examining the role of microorganisms in impaired chronic wound healing. Adv Wound Care (New Rochelle). 2014;3(7):502-10.
43. Chang ZM, Wang Z, Lu MM, Shao D, Yue J, Yang D, et al. Janus silver mesoporous silica nanobullets with synergistic antibacterial functions. Colloid Surface B. 2017;157:199-206.
44. Liston SD, Willis LM. Racing to build a wall: glycoconjugate assembly in Gram-positive and Gram-negative bacteria. Curr Opin Struct Biol. 2021;68:55-65.
45. Megrian D, Taib N, Witwinowski J, Beloin C, Gribaldo S. One or two membranes? Diderm Firmicutes challenge the Gram-positive/Gram-negative divide. Mol Microbiol. 2020;113(3):659-71.
46. Ran P, Chen WJ, Zheng H, Zhou JJ, Qiu B, Cao WX, et al. Surface decoration of black phosphorus nanosheets to generate oxygen and release $^1O_2$ for photodynamic killing of bacteria. Nanoscale. 2021;13(31):13506-18.

Scheme

Scheme 1 is available in the Supplementary Files section.

Figures

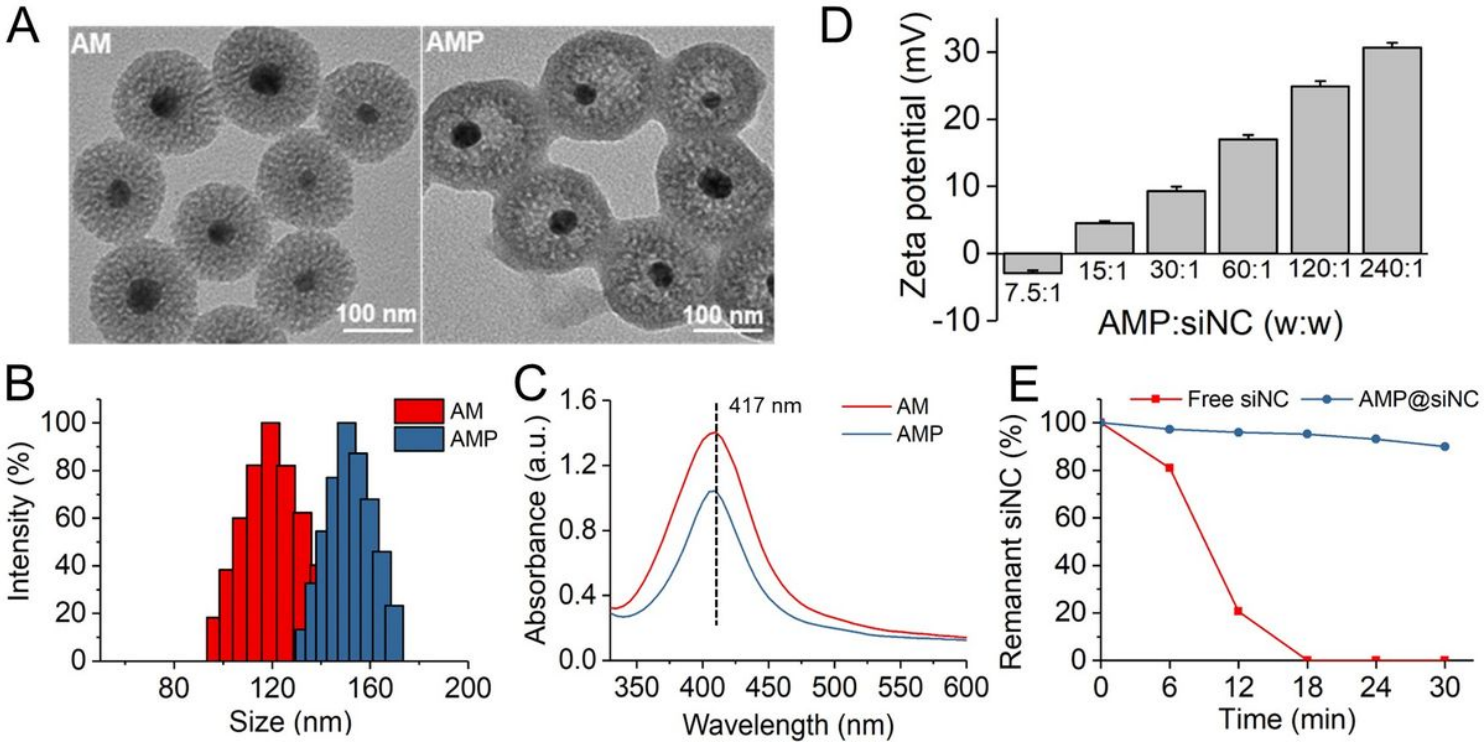

Figure 1

Characterization of AMP@siRNA. **(A)** TEM images, **(B)** The hydrodynamic size, and **(C)** the UV-vis absorption spectrum of AM and AMP. **(D)** Zeta potential of AMP@siNC at different weight ratios, n = 3. **(E)** Quantitative analysis of remnant siNC of free siNC and AMP@siNC after incubation with RNase A-containing solution for a predetermined time by Image J software.

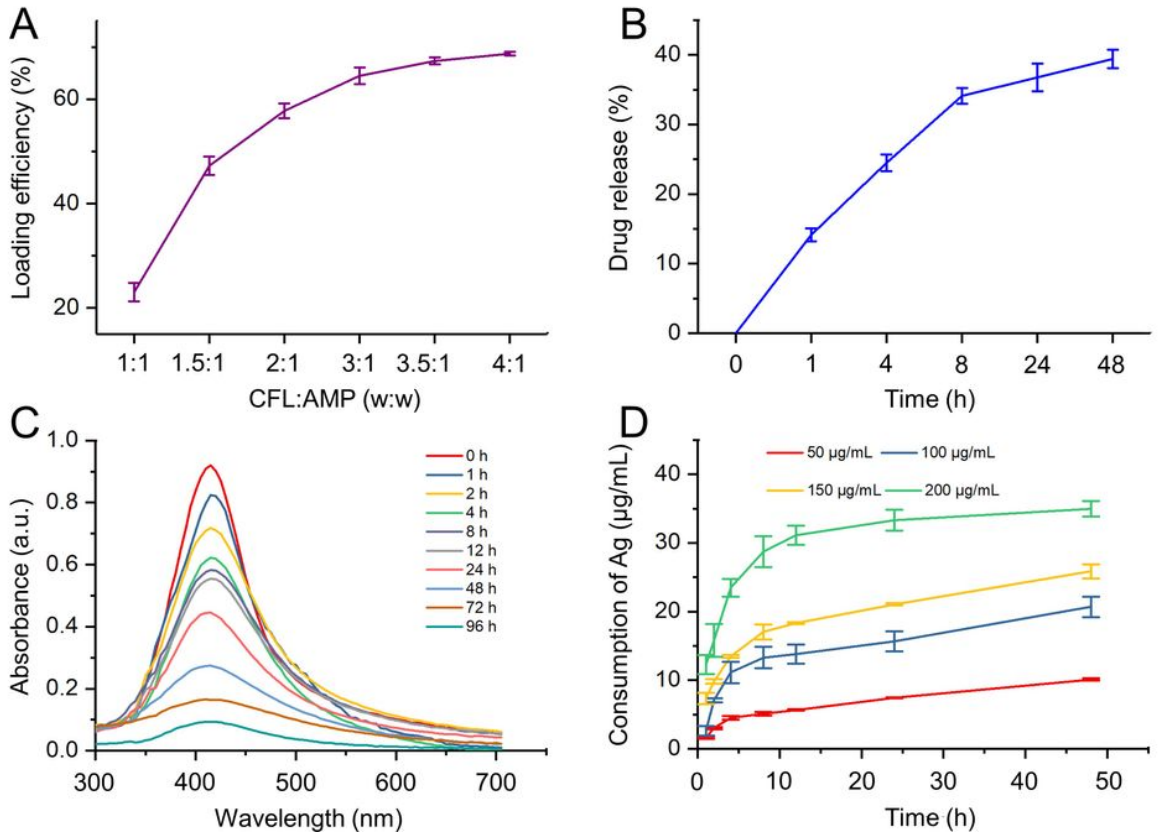

Figure 2

The loading and release profiles of antibacterial components. **(A)** The loading efficiency of ciprofloxacin (CFL) of AMP at different weight ratios. **(B)** Cumulative release profiles of CFL from AMPC in PBS (pH 7.4) at 37°C. **(C)** The UV-vis spectra and **(D)** consumption of Ag from AMPC with different concentrations over time in LB medium at 37°C.

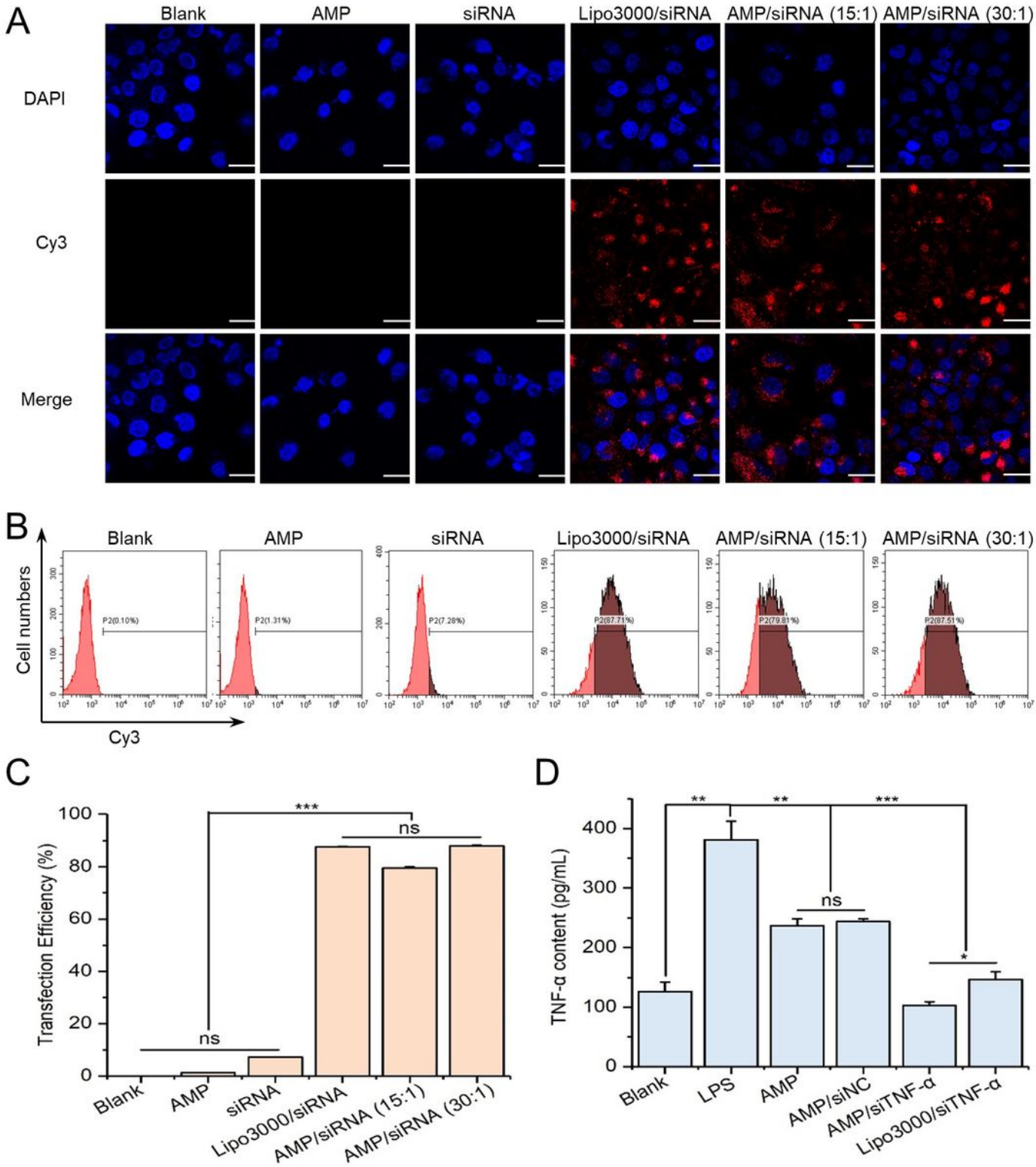

Figure 3

AMP-mediated siRNA transfection and gene silencing in RAW264.7 cells. **(A)** Fluorescence microscopy images of RAW264.7 cells treated with different formulations. Cell nuclei are stained with DAPI (blue). siRNA is labeled with Cy3. Thus, the intracellular siRNA will present red fluorescence signal. Scale bar = 20 μm. **(B)** Cell histograms and **(C)** transfection efficiencies for evaluating the siRNA delivery effect by flow cytometry. **(D)** The expression levels of TNF-α protein in RAW264.7 cells treated with different

formulations were evaluated by the TNF-α ELISA kit. The data are calculated by mean ± SD, n = 3 (*, $p < 0.05$; **, $p < 0.01$; ***, $p < 0.001$).

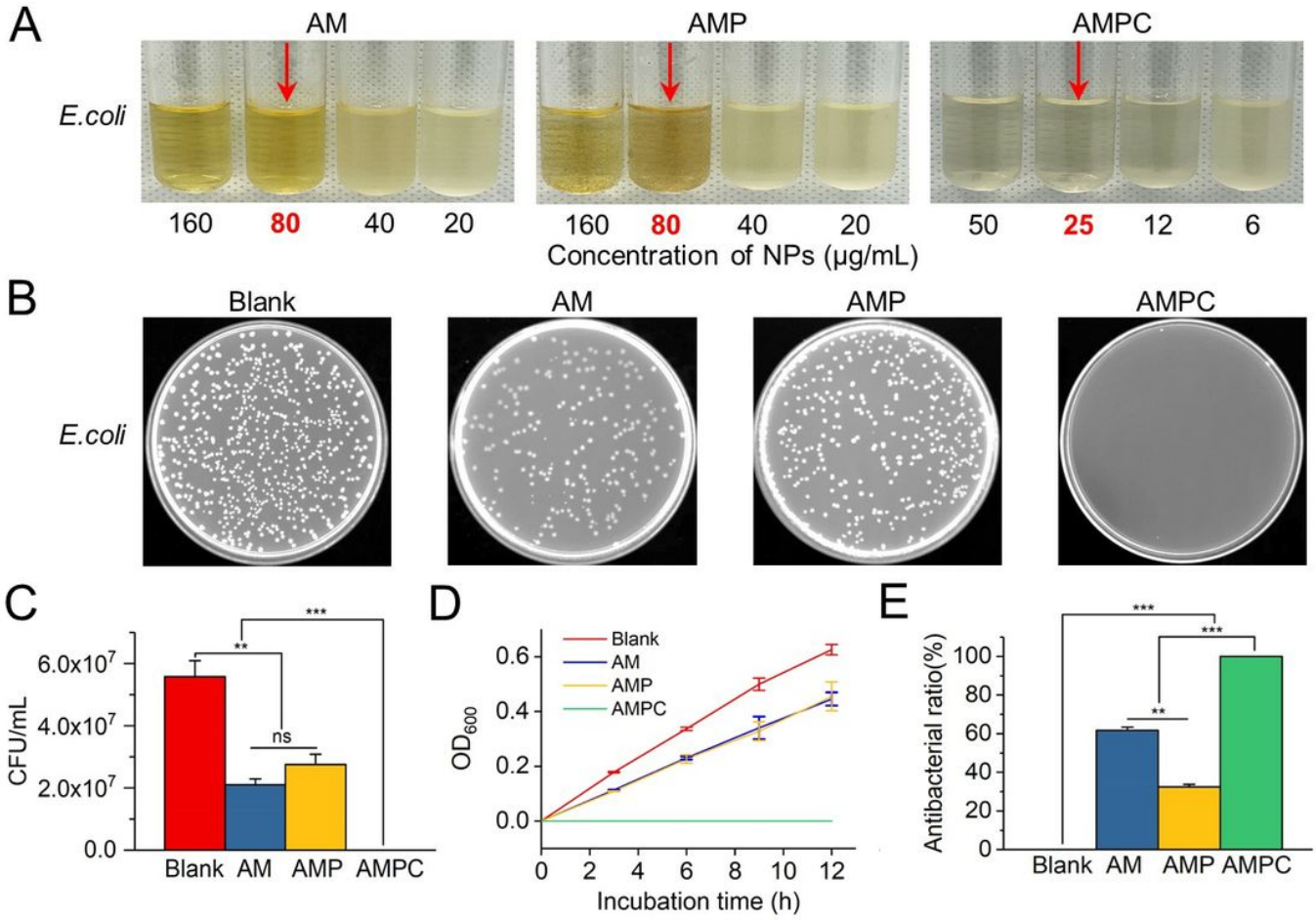

Figure 4

In vitro evaluation of the antibacterial activity of NPs. **(A)** The turbidity observation of *E. coli* in LB medium treated with different concentrations of formulations (AM, AMP, and AMPC). The MICs of the sample are marked with a red arrow. **(B)** The photographs of *E. coli* colony on agar plates, **(C)** quantitative bacterial colonies densities based on **(B)**, **(D)** growth curve, and **(E)** antibacterial ratio of *E. coli* in logarithmic growth period treated with different NPs for 12 h. The data represent mean ± SD, n = 3 (*, $p < 0.05$; **, $p < 0.01$; ***, $p < 0.001$).

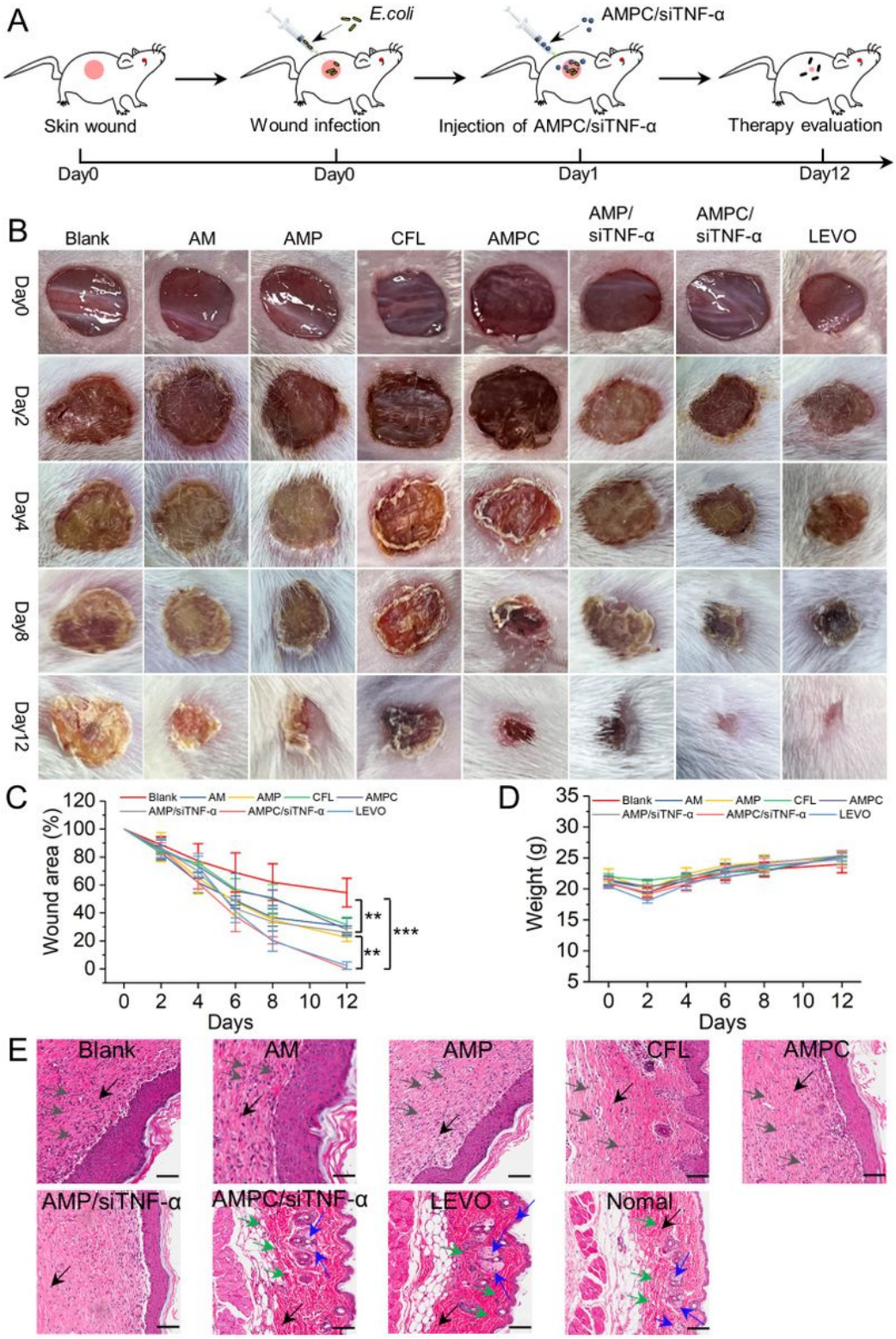

Figure 5

In vivo wound healing efficacy after being treated with different formulations. **(A)** The schematic diagram for the *in vivo* treatment evaluation procedure. **(B)** The photographs of *E. coli*- infected skin wound images treated with AM, AMP, CFL, AMPC, AMP/siTNF-α, AMPC/siTNF-α, and LEVO. **(C)** Closed area ratio of infected wounds (**, $p < 0.01$; ***, $p < 0.001$). **(D) The** change profiles of mouse weight treated with different formulations. **(E)** Histological graphs of skin tissue by H&E staining. Scale bar = 100 μm. Black,

gray, green, and blue arrows indicate cell nucleus, neutrophils and inflammatory cells, fibroblasts, and sebaceous glands, respectively.

Supplementary Files

This is a list of supplementary files associated with this preprint. Click to download.

- SupportingInformation.docx
- floatimage1.jpeg
- floatimage2.jpeg